Supplement of Atmos. Chem. Phys., 21, 13713–13727, 2021
https://doi.org/10.5194/acp-21-13713-2021-supplement

Atmospheric Chemistry and Physics
Open Access
EGU

Supplement of

A comprehensive observation-based multiphase chemical model analysis of sulfur dioxide oxidations in both summer and winter

Huan Song et al.

Correspondence to: Keding Lu (k.lu@pku.edu.cn)

This PDF file includes:

Supplementary text

Figures S1 to S9

Tables S1 to S9

SI References

Supplementary Information Text

Text S1. Activity coefficients of main reactants in the PKU-MARK model

The properties of electrolytes play an important role in the kinetic salt effect in the aqueous phase reaction. Atmospheric heterogeneous reactions occurring in aerosol deliquescent particles are characterized by high ionic strength (I_s). In these multicomponent mixture, reaction rates should be replaced by the activity coefficient, which representing the thermodynamic non-ideality caused by all-molecular interactions (Rusumdar et al., 2016;Rusumdar et al., 2020). Suitable multiphase chemistry models should apply activity coefficients instead of reaction rate constants in non-ideal solution. Heterogeneous processed in clouds and haze may be considered as occurring in dilute electrolytes and there is no need to consider the influence of ionic strength, this is not the case for high ionic strength deliquescent particles. Based on the measurement of ambient aerosol deliquescent particles (Herrmann et al., 2015), in marine areas, the ionic strength is about 6 M and in urban environments can reach about 8-18 M. Fountoukis and Nenes using the ISORROPIA–II model predicted high levels of ionic strength ranging between 13 and 43 M during the severe Beijing Haze (Fountoukis and Nenes, 2007a). In some extreme cases, the ionic strength of aerosol deliquescent particles can even reach 100 M (Cheng et al., 2016a). In two field campaign mentioned in this study, the mean value of ionic strength is 56.55 ± 39.83 M (±1σ) in winter and 24.26 ± 13.3 M (±1σ) in summer in haze periods ($PM_{2.5}$>75μg/m^3), and in extremely situation, 175.45 M in winter and 96.41 M in summer. In these cases, large errors can be introduced in the model calculation without considering the influence of ionic strength on aqueous phase reaction rate and heterogeneous mass transport.

Several studies are developed to evaluate the effects of ionic strength on the activity of aqueous phase ions and organic matters (Pitzer, 1991;Li et al., 1994;Polka et al., 1994;Ming and Russell, 2002;Raatikainen and Laaksonen, 2005;Clegg et al., 2008;Zuend et al., 2008;Zuend et al., 2011), and during the latest year considerable effort has been devoted to developing kinetic model frameworks for the modelling of processes in multicomponent atmospheric particles, which include both a detailed description of organic and inorganic multiphase chemistry as well as detailed thermodynamic comprehensions of its non-ideal behavior (Rusumdar et al., 2016). In this study, the activity coefficients of TMI were calculated by the Extended

Debye-Hückel equation (Ross and Noone, 1991;Linder and Murray, 1982;Kontogeorgis et al., 2018). Other ions and organic oxalic acid and its complexes used the typical values predicted by AIOMFAC model by Rusumdar (Rusumdar et al., 2020). As for neutral solutes which activity coefficients are not corrected in AIOMFAC model, such as O_3, O_2 and small molecules OH and HO_2, logarithm of the activity coefficient of neutral solutes is a linear function of the effective ionic strength and the Sechenov coefficient (Rischbieter et al., 2000;Beltran, 2003;Clever, 1983;Ross and Noone, 1991). Unfortunately, Setchenov parameters are unknown for H_2O_2, which is an important source of aqueous OH radical and other ROS. Several studies(Ali et al., 2014;Cheng et al., 2016b;Liu et al., 2020) showed that the formation rate of S(VI) by H_2O_2 increases with aerosol condensed phase solution ionic strength and proposed different expression with the limitation of maximal ionic strength equal to 5 M. In this case, considering the high value of ionic strength in the two field campaigns (averaged values are beyond 5 M), direct extrapolation of the observed/predicted *a-I* relationship into such high ranges of ionic strength may not be appropriate. Thus, in this paper, the activity coefficient of H_2O_2 is only considered when calculating the sulfate formation rate. Corresponding typical activity coefficient values and calculation expressions are summarized in **Table S2 and S3**. The influence of ionic strength on gas phase molecular Henry's law coefficients were also considered in the MARK model which are summarized in **Table S3**.

Text S2. The concentration of aerosol particle transition metals in urban areas

For the lack of Mn concentration in $PM_{2.5}$ during two field campaigns, we summarized the concentration of transition metals in urban areas, mainly in Beijing winter in **Table S9**. The mass concentration ratio of Fe/Mn is in the range of 8.6 to 31 in Beijing, and can up to 78 in India. In the calculation of sulfate formation, we used the mass concentration ratio of Fe/Mn as 28 which is a medium value of the ratios. The modeled ratio of soluble Fe (III) to total Fe in the whole winter field campaign was in the range of 0.02% to 27.63% with an average value of 1.63% and in the range of 0.04% to 3.29% with an average value of 0.79% in polluted and highly polluted conditions. The modeled ratio of soluble Mn (II) to total Mn in the whole winter field campaign was in the range of 0.01% to 97.21% with an average value of 21.78% and in the range of 0.01% to 80.46% with an average value of 19.83% in polluted and highly polluted conditions.

Text S3. Four haze periods in PKU-17 observation

Fig. S4 shows the diurnal trends of the key parameters measured in the PKU field campaign for four haze periods. All four haze periods lasted for 6 days. Due to the strict emission control policies enacted by the Chinese government, the concentration of $PM_{2.5}$ decreased compared to the same period in 2016 while still cause severe haze pollution in 2017. H_2O_2 exhibited a typical diurnal pattern with a maximum in the afternoon and low concentrations in the morning and night. It was worth mentioning that some studies reported high H_2O_2 concentrations during haze episodes, while in our study the average

concentration of H_2O_2 was only about 0.02 ppb. Low OH radicals and O_3 concentrations indicated low photochemical activity. The largest $PM_{2.5}$ concentrations of period IV and II were observed exceeding 150 μg/m^3, which was coincident with higher concentrations of transition metal including Fe and Cu. Period IV was characterized by lower gas-phase H_2O_2 and higher RH as well as higher aerosol liquid water content compared to the other three periods. Due to the lack of OH radical data during Period IV, averaged OH concentrations from the other three haze periods were used in the calculation causing small biases due to the reduced gas-phase oxidant pathway during the haze period. Period II was characterized with the highest SO_2 concentration which was beneficial to the formation of secondary sulfate aerosol. The other two haze periods including Period I and Period III also own high levels of 24-hour averaged $PM_{2.5}$ loading exceeding 75 μg/m^3. However, according to the observed SO_4^{2-} concentration, high concentrations of sulfate only appeared in the fourth stage of pollution indicating the importance of RH and aerosol TMI.

Figures

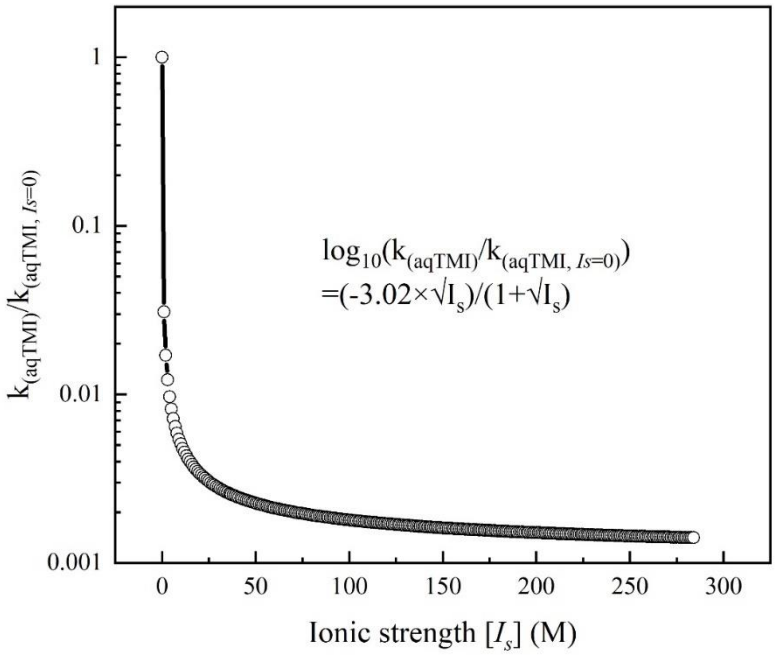

Fig. S1. Ionic strength of aerosol particle solution influence on the aqTMI rate constant.

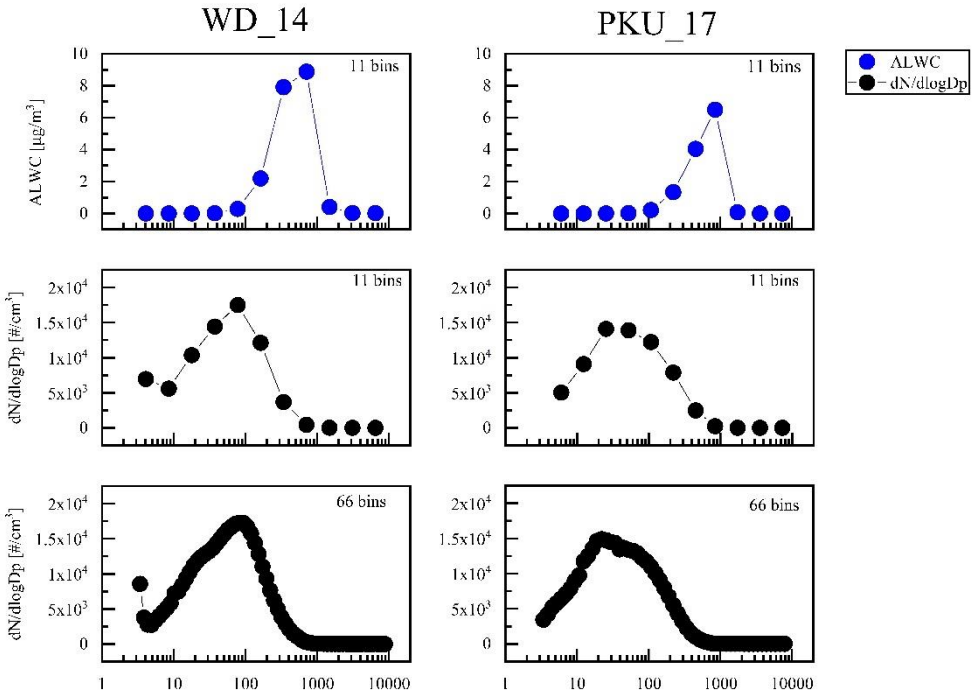

Fig. S2. Distribution of ALWC and number concentration with aerosol particle bins in two campaigns.

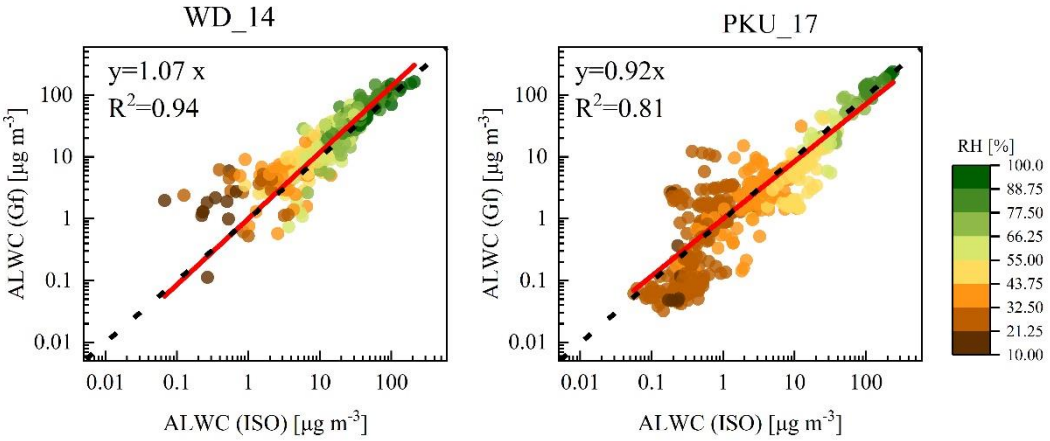

Fig. S3. Calculated aerosol water by ISORROPIA-II model and H-TDMA method in two field campaigns during haze periods. The plots were colored with the relative humidity values. The black dashed line in the figure is the 1:1 baseline, and the red solid line is the linear fitting result assuming the intercept is zero.

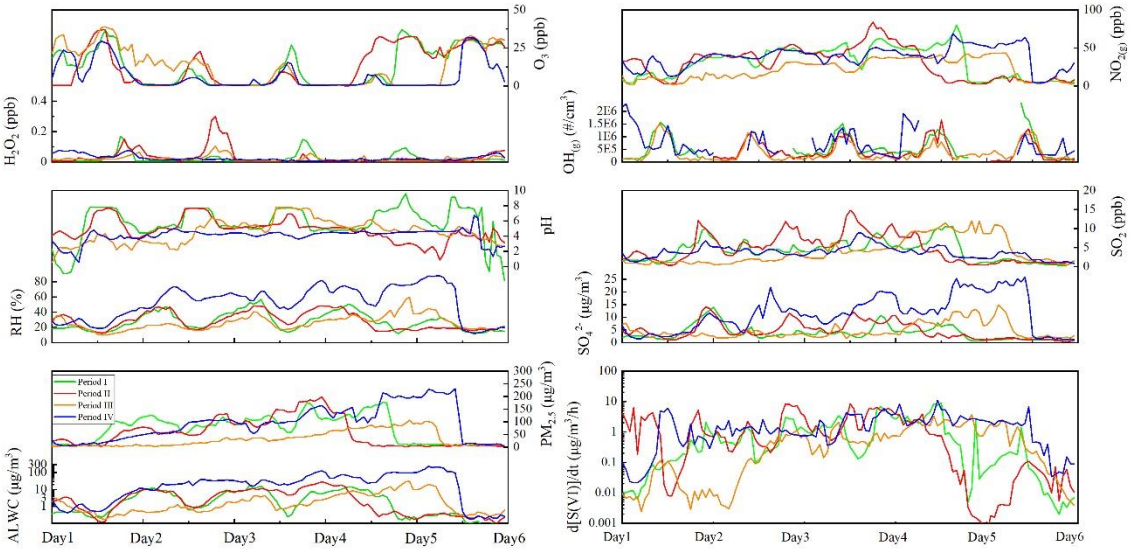

Fig. S4. Time series of observed gas-phase pollutants concentrations, RH, Temperature, $PM_{2.5}$ mass loading and calculated aerosol pH and water content and sulfate formation rates in these four haze periods in PKU-17 field campaign.

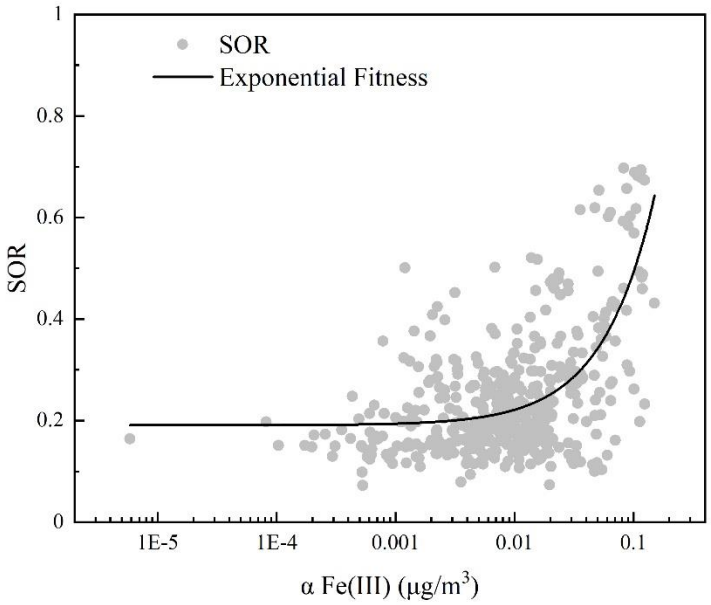

Fig. S5. SOR ($\equiv n(SO_2)/n(SO_2+SO_4^{2-})$) correlations with effective Fe (III) concentrations in PKU-17 winter field campaign.

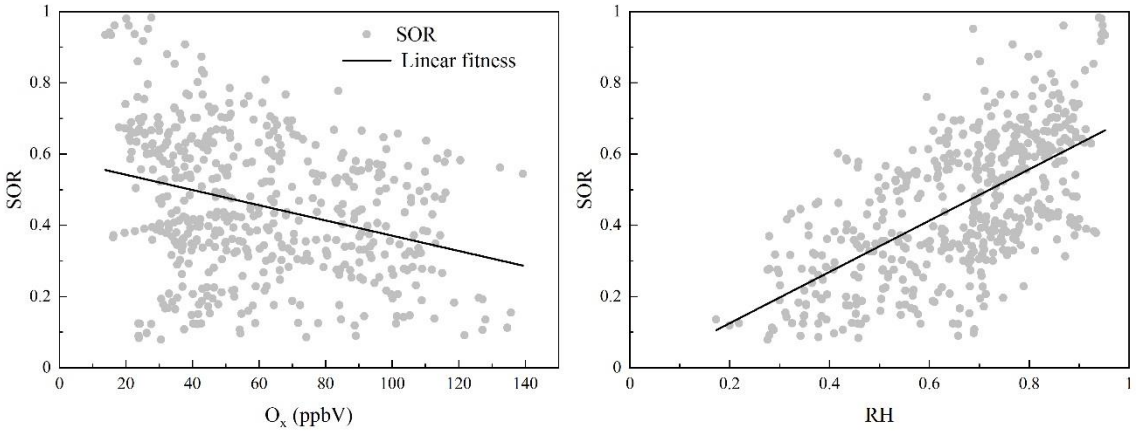

Fig. S6. SOR ($\equiv n(SO_2)/n(SO_2+SO_4^{2-})$) correlations with odd oxygen ($[O_x] \equiv [O_3]+[NO_2]$) and relative humidity (RH) in WD-14 summer field campaign.

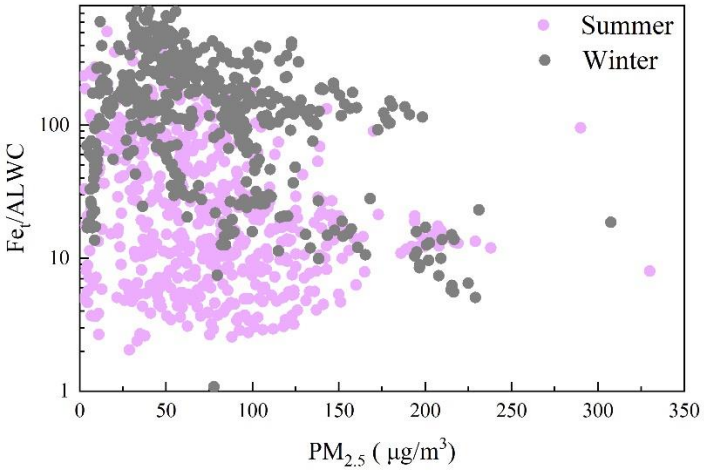

Fig. S7 The "dilution effect" of Fe mass concentration and ALWC increasing with PM mass in winter and summer.

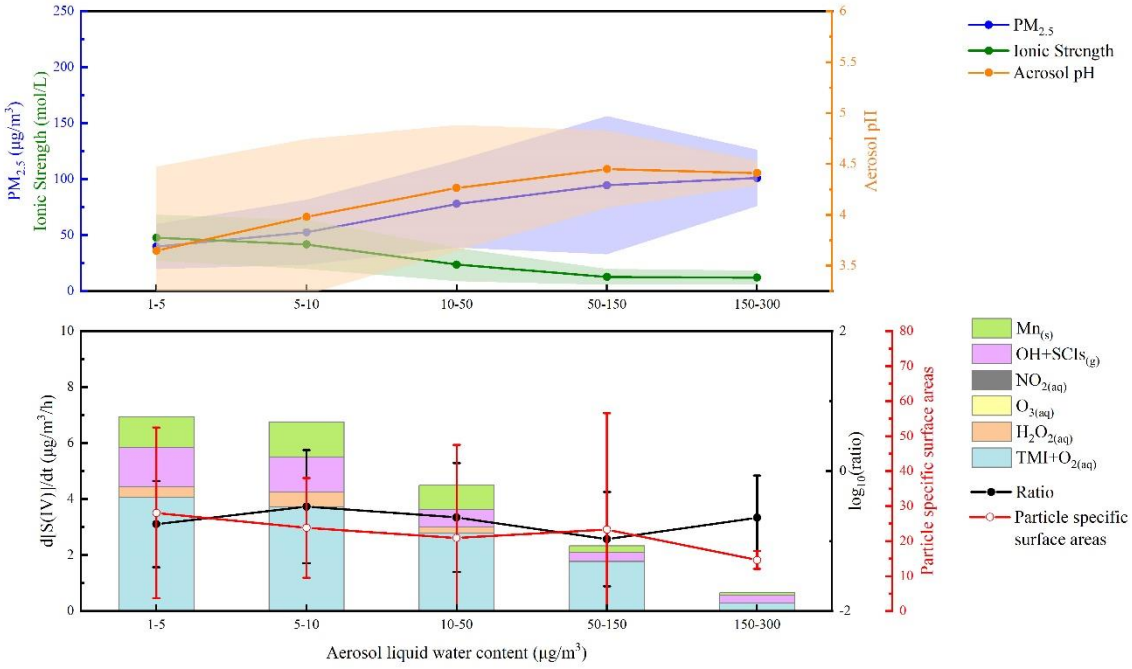

Fig. S8. Variation of $PM_{2.5}$, ionic strength, aerosol pH, particle specific surface areas and sulphate formation rates from different pathways with aerosol liquid water content (ALWC) during summer field campaign.The total number of valid data points shown in the figure is 501. The shaded area refer to the error bar (±1 σ) of $PM_{2.5}$ mass concentration, aerosol ionic strength and pH calculated by ISORROPIA-II(Fountoukis and Nenes, 2007b). Ratio in the second panel refers to the ratio of contributions from Mn-surface and aqTMI to produce sulphate. Particle specific surface areas represent the ratio of particle surface area (μm^2/cm^3) and mass concentration (μg/m^3).

Tables

Table S1. Reaction rate expression and constant for SO2 oxidation by OH in the gas-phase.

Oxidant	The reaction rate expression and constant [a]	References
OH	$R_{SO2+OH} = k_0[SO_2(g)][OH(g)]$	Burkholder et al. (2020)
	$k_{0low} = 3.3\times10^{-31}\times(T/300K)^{-4.3}$ cm^6 s^{-1}	
	$k_{0high} = 1.6\times10^{-12}$ cm^3 s^{-1}	
	$F_c = 0.6$	

[a] We report the low and the high pressure limit of k for SO_2 oxidation by OH. F_c is used to calculate the dependence of k on pressure and temperature (details see the reference(Burkholder et al., 2020)).

Table S2. Aqueous-phase reaction rate expressions, rate constants (k) and influence of ionic strength (Is) on k for sulfate production in aerosol particle condensed phase.

Oxidants	The reaction rate expressions ($R_{S(IV)+oxi}$), constants (k) and influence of I_s (in unit of M) on k [a]	Notes	References
O_3	$(k_1[H_2SO_3] + k_2[HSO_3^-] + k_3[SO_3^{2-}])\,[O_3(aq)]$		Seinfeld and Pandis (2016)
	$k_1 = 2.4\times10^4\ M^{-1}\ s^{-1}$		
	$k_2 = 3.7\times10^5\times e^{(-5530\times(1/T-1/298))}\ M^{-1}\ s^{-1}$		
	$k_3 = 1.5\times10^9\times e^{(-5280\times(1/T-1/298))}\ M^{-1}\ s^{-1}$		
	$\log_{10}(\frac{k}{k^{I_s=0}}) = b_1\left(\frac{\sqrt{I_s}}{1+\sqrt{I_s}} - 0.3I_s\right)$	$I_{s,\,max}$ = 0.94 M	Maahs (1983)
	b_1 is in range of 0.7 to 1.3 [b]		
	$\frac{k}{k^{I_s=0}} = 1 + b_2 I_s$	$I_{s,\,max}$ = 1.2 M	Lagrange et al. (1993)
	b_2 is in range of 1.34 to 6.13 [b]		
H_2O_2	$k_4[H^+][HSO_3^-][H_2O_2(aq)]/(1+K[H^+])$		McArdle and Hoffmann (1983)
	$k_4 = 7.45\times10^7\times e^{(-4430\times(1/T-1/298))}\ M^{-1}\ s^{-1}$		
	$K = 13\ M^{-1}$		
	$\log_{10}(\frac{k}{k^{I_s=0}}) = 0.36I_s - \frac{1.018\sqrt{I_s}}{1+0.17\sqrt{I_s}}$	$I_{s,\,max}$ = 5 M	Maaß et al. (1999)
	$ln(\frac{k}{k^{I_s=0}}) = 30.374 - \frac{6824.2068}{215.365+I_s}$ [c]		Liu et al. (2020)
NO_2	$k_5[S(IV)]\,[NO_2(aq)]$ [d]		Clifton et al. (1988);Lee and Schwartz (1983)
	$k_{5low} = 2\times10^6\ M^{-1}\ s^{-1}$		
	$k_{5high} = (1.24–2.95)\times10^7\ M^{-1}\ s^{-1}$		
	$\log_{10}(\frac{k}{k^{I_s=0}}) = b_3 I_s$	Theoretical prediction	Cheng et al. (2016b)
	$b_3 > 0$ [e]		
TMI+O_2 [f]	$k_6[H^+]^{-0.74}[S(IV)][Mn(II)][Fe(III)]$ (pH ≤ 4.2)		Ibusuki and Takeuchi (1987)
	$k_6 = 3.72\times10^7\times e^{(-8431.6\times(1/T-1/297))}\ M^{-2}\ s^{-1}$		
	$k_7[H^+]^{0.67}[S(IV)][Mn(II)][Fe(III)]$ (pH > 4.2)		
	$k_7 = 2.51\times10^{13}\times e^{(-8431.6\times(1/T-1/297))}\ M^{-2}\ s^{-1}$		
	$\log_{10}(\frac{k}{k^{I_s=0}}) = \frac{b_4\sqrt{I_s}}{1+\sqrt{I_s}}$ [g]	$I_{s,\,max}$ = 2 M	Martin and Hill (1987, 1967)
	b_4 is in range of –4 to –2		

Mn surface	$k_8 \times f(H^+) \times f(T) \times f(I_s) \times [\mathrm{Mn(II)}] \times [\mathrm{SO_2(g)}] \times \mathrm{A}$ k_8=11079.30 μg/m^3/min, A is the surface area concentration in nm^2/cm^3, and the SO_2 mixing ratio is in ppbV $f(H^+)$=-1/(1-8.83×10^{17}×[H$^+$]-7.84×10^{21}×[H$^+$]) $f(T)$=e$^{-11576.08\times(1/T-1/298)}$ $f(I_s) = \begin{cases} 1, I_s < 1.52911 \times 10^{-41} \times e^{\frac{T}{2999.19}} + 13.8704 \\ 10.3, I_s \geq 1.52911 \times 10^{-41} \times e^{\frac{T}{2999.19}} + 13.8704 \end{cases}$	Wang et al. (2020)
Nitrate photolysis	$1.64 \times EF \times [NO_3^-] \times J_{HNO3} \times \frac{K_{HONO}}{K_{HONO}+[H^+]} \times v \times A \times 0.25 \times [SO_2]$ KHONO=10$^{-3.3}$ M, EF= 1~100	Zheng et al. (2020)

[a] The aerosol pH was in the range of 4.1 to 5.2 based on the calculations of ISORRPIA II model in winter and 3.8 to 4.9 in summer, which are consistent with the observed in NCP (Liu et al., 2017;Guo et al., 2017).

[b] The values of b_1 and b_2 are different for different solutions (Maahs, 1983; Lagrange et al., 1994). Since these values vary largely and have a significant impact on the estimated reaction rate at high I_s in aerosol water, we used a medium value of b_1=1.0 and b_2=1.94 in according to the calculation in Cheng to show the general pattern. Due to the low concentration of O_3 during haze periods, the pathway provides little contribution in the sulfate formation.

[c] The last expression is the fitting results from the measurement results of Liu et al. (2020) Figure S10. The typical enhancement factor of proton-catalyzed sulfate formation rate is 40 in the haze periods of the winter campaign with an averaged ionic strength as 36.3 M.

[d] The k_{5low} was taken from Lee and Schwartz (1983). They reported a lower-limit value of k_{5low} = 2×10^6 M^{-1} s^{-1} at pH of 5.8 and 6.4. The k_{5high} is in the pH range of 5.3–13 as reported by Clifton et al. (1988) and it increases with increasing pH. We used the value k_{5high} = 1.24×10^7 M^{-1} s^{-1} for pH < 5.3, and k_{5high} = (0.1239 pH+0.5954) ×10^7 M^{-1} s^{-1} for pH in 5.3–7.8 in the present calculations.

[e] The b_3 was predicted theoretically to be positive as 0.5 (Cheng et al., 2016b), however, no specific value of b_3 was determined from laboratory work. Because of the high value of ionic strength during the PKU campaign, we proposed an expression for the activity coefficient of NO_2 based on the Sechenov theory to reflect the trend of its reaction rate increasing with the concentrations and chose *b3* value as 0.01, typical value of activity enhancement of NO_2 with S(IV) is 2.31 with averaged ionic strength equaling to 36.3 during the haze periods. With *b3* equaling to 0.5 proposed in Cheng et al. (2016b), however, typical value is 1.41 × 10^{18}.

Thus we didn't consider the influence of I_s on S(IV) + NO_2 in aerosol water in our calculation.

[f] S(IV) oxidation by O_2, which is via a radical chain mechanism, can be initiated by transition metal ions (TMIs) in bulk water (k_6 and k_7). In our calculation, the reaction rate k_6 and k_7 was used for sulfate production via S(IV) + O_2. Only Fe (III) and Mn (II) are considered here, since other transition metal ions (TMIs), such as Sc (III), Ti (III), V(III), Cr (III), Co (II), Ni (II), Cu

(II) and Zn (II), showed much less catalytic activities (Huss Jr et al., 1982). In addition, it has been concluded that the decreased temperature would generally lead to a decrease in overall reaction rate. Based on the measurement results of Ibusuki and Takeuchi (1987), the correction of temperature are considered in the present study.

[g] Impact of ionic strength on the sulfate formation rate of aqueous phase TMI-catalyzed oxidation of dissolved SO_2 by O_2 in aerosol particles was studied by Liu et al. (2020). In their results, b_4 is -3.02 based on the fitting modeling and in the range of -2 for Fe(III) and -4 for Mn(II) (Martin and Hill, 1987, 1967). We used b_4 as -3.02 in the calculations in the present study.

145 Table S3. Calculations of Henry' law coefficients and influence of ionic strength.

Gas species	Henry's law coefficient and the influence of I_s	Notes	References
SO_2	$H_{SO_2}^{I_s=0} = 1.23 \times e^{(3145.3\times(\frac{1}{T}-\frac{1}{298}))}$		Seinfeld and Pandis (2016)
	$\log_{10}(\frac{H_{SO_2}}{H_{SO_2}^{I_s=0}}) = (\frac{22.3}{T} - 0.0997) \times I_s$	$I_{s,\,max}$ = 6 M	Millero et al. (1989)
O_3	$H_{O_3} = e^{(\frac{2297}{T}-2.659\times I_s+688\times\frac{I_s}{T}-12.19)}$	$I_{s,\,max}$ = 0.6 M	Kosak-Channing and Helz (1983)
H_2O_2 [b]	$H_{H_2O_2}^{I_s=0} = 1.3 \times 10^5 \times e^{(7297.1\times(\frac{1}{T}-\frac{1}{292}))}$		Seinfeld and Pandis (2016);Chung et al. (2005)
	$\frac{H_{H_2O_2}}{H_{H_2O_2}^{I_s=0}} = 1 - 1.414 \times 10^{-3} I_s^2 + 0.121 I_s$	$I_{s,\,max}$ = 5M	Liu et al. (2020)
NO_2 [a]	$H_{NO_2}^{I_s=0} = 1.0 \times 10^{-2} \times e^{(2516.2\times(\frac{1}{T}-\frac{1}{298}))}$		Seinfeld and Pandis (2016)

[a] We didn't consider the influence of I_s on H_{NO2} in our calculation due to the lack of relevant laboratory data. H is in unit of M atm^{-1}.

Table S4. Typical activity coefficient values and expressions used in the MARK model

Species	Calculation expression or typical value
Inorganic ions	
H^+	0.4
OH^-	0.5
NH_4^+	0.2
Na^+	0.3
SO_4^{2-}	0.02
HSO_4^-	1
NO_3^-	0.4
Fe(II), Cu(I), Cu(II), Mn(II) ions and their hydroxides	$\log_{10}(a_i) = \frac{-z_i^2 \times 0.5109\sqrt{I_s}}{1 + 1.5 \times \sqrt{I_s}}$
Fe(III) and its hydroxides	0.001
Organic matters and Fe-complex	
$H_2C_2O_4$	0.6
$HC_2O_4^-$	0.05
$C_2O_4^{2-}$	0.43
$[Fe(C_2O_4)_2]^-$	0.43
$[Fe(C_2O_4)]^+$	0.43
$[Fe(C_2O_4)_3]^{3-}$	0.001

[a] Non-ideality is treated with the approach by Zuend et al. (2008);Zuend et al. (2011) applied in the AIOMFAC model (Aerosol Inorganic–Organic Mixtures Functional groups Activity Coefficients, http://www.aiomfac.caltech.edu/index.html, last access: 18 July 2020).

Table S5. Kinetic data for the simulation of reactions in the aerosol particle condensed phase.

Number	Reaction	k_{298} (M^{-n+1} s^{-1})	Ea/R (K)
Iron reactions			
A1	$Fe^{2+} + H_2O_{2(a)} \rightarrow Fe^{3+} + OH_{(a)} + OH^-$	70	5050
A2	$Fe^{2+} + O_{3(a)} \rightarrow FeO^{2+} + O_{2(a)}$	8.2×10^5	4690
A3	$FeO^{2+} + H_2O_{2(a)} \rightarrow Fe^{3+} + HO_{2(a)} + OH^-$	9.5×10^3	2766
A4	$FeO^{2+} + HO_{2(a)} \rightarrow Fe^{3+} + O_{2(a)} + OH^-$	2×10^6	0
A5	$FeO^{2+} + OH_{(a)} + H^+ \rightarrow Fe^{3+} + H_2O_{2(a)}$	1×10^7	0
A6	$FeO^{2+} + H_2O_{(a)} \rightarrow Fe^{3+} + OH_{(a)} + OH^-$	2.3×10^{-2}	4100
A7	$FeO^{2+} + Fe^{2+} + H_2O_{(a)} \rightarrow 2\ Fe^{3+} + 2\ OH^+$	7.2×10^4	842
A8	$FeO^{2+} + Fe^{2+} + H_2O_{(a)} \rightarrow Fe(OH)_2Fe^{4+}$	1.8×10^4	5052
A9	$Fe(OH)_2Fe^{4+} + 2\ H^+ \rightarrow 2\ Fe^{3+} + 2\ H_2O_{(a)}$	2	5653
A10	$Fe(OH)_2Fe^{4+} \rightarrow 2\ Fe^{3+} + 2\ OH^-$	0.49	8780
A11	$FeO^{2+} + HNO_{2(a)} \rightarrow Fe^{3+} + NO_{2(a)} + OH^-$	1.1×10^4	4150
A12	$FeO^{2+} + H^+ + NO_2^- \rightarrow Fe^{3+} + NO_{2(a)} + OH^-$	2.5×10^5	0
A13	$FeO^{2+} + HSO_3^- \rightarrow Fe^{3+} + OH^- + SO_3^-$	1×10^5	0
A14	$Fe^{2+} + OH_{(a)} \rightarrow Fe(OH)^{2+}$	4.3×10^8	1100
A15	$Fe(OH)^{2+} + HO_{2(a)} \rightarrow Fe^{2+} + O_{2(a)} + H_2O_{(a)}$	1.3×10^5	0
A16	$Fe(OH)^{2+} + O_2^- \rightarrow Fe^{2+} + O_{2(a)} + OH^-$	1.5×10^8	0
A17	$Fe^{3+} + O_2^- \rightarrow Fe^{2+} + O_{2(a)}$	1.5×10^8	0
A18	$Fe^{2+} + 2\ H^+ + O_2^- \rightarrow Fe^{3+} + H_2O_{2(a)}$	1×10^7	0
A19	$Fe^{2+} + HO_{2(a)} + H^+ \rightarrow Fe^{3+} + H_2O_{2(a)}$	1.2×10^6	5050
A20	$Fe(OH)_2^+ + O_2^- \rightarrow Fe^{2+} + O_{2(a)} + 2\ OH^-$	1.5×10^8	0
A21	$Fe(OH)^{2+} + HSO_3^- \rightarrow Fe^{2+} + SO_3^- + H_2O_{(a)}$	30	0
A22	$Fe^{2+} + SO_5^- + H_2O_{(a)} \rightarrow Fe(OH)^{2+} + HSO_5^-$	2.65×10^7	5809
A23	$Fe^{2+} + HSO_5^- \rightarrow Fe(OH)^{2+} + SO_4^-$	3×10^4	0
A24	$Fe^{2+} + SO_4^- \rightarrow Fe^{3+} + SO_4^{2-}$	4.6×10^9	-2165
A25	$Fe^{2+} + S_2O_8^{2-} \rightarrow Fe^{3+} + SO_4^- + SO_4^{2-}$	17	0
Copper reactions			
A26	$Cu^+ + 2\ H^+ + O_2^- \rightarrow Cu^{2+} + H_2O_{2(a)}$	8×10^9	0

A27	$Cu^{+} + HO_{2(a)} + H^{+} \rightarrow Cu^{2+} + H_2O_{2(a)}$	2.2×10^{9}	0
A28	$Cu^{+} + OH_{(a)} \rightarrow Cu^{2+} + OH^{-}$	3×10^{9}	0
A29	$Cu^{2+} + HO_{2(a)} \rightarrow Cu^{+} + H^{+} + O_{2(a)}$	1×10^{8}	0
A30	$Cu^{2+} + O_2^{-} \rightarrow Cu^{+} + O_{2(a)}$	1×10^{9}	0
A31	$Cu^{+} + O_{2(a)} \rightarrow Cu^{2+} + O_2^{-}$	4.6×10^{5}	0
A32	$Cu^{+} + H^{+} + O_{3(a)} \rightarrow Cu^{2+} + O_{2(a)} + OH_{(a)}$	3×10^{7}	0
A33	$Cu^{+} + H_2O_{2(a)} \rightarrow Cu^{2+} + OH_{(a)} + OH^{-}$	7×10^{3}	0
A34	$Cu^{+} + SO_4^{-} \rightarrow Cu^{2+} + SO_4^{2-}$	3×10^{8}	0
Mn reactions			
A35	$Mn^{4+} + H_2O_{2(a)} \rightarrow Mn^{2+} + O_{2(a)} + 2H^{+}$	7.3×10^{4}	0
A36	$Mn^{3+} + H_2O_{2(a)} \rightarrow Mn^{2+} + HO_{2(a)} + H^{+}$	7.3×10^{4}	0
A37	$MnOH^{2+} + H_2O_{2(a)} \rightarrow MnO_2^{+} + H^{+}$	2.8×10^{3}	0
A38	$MnO_2^{+} + HO_{2(a)} + H^{+} \rightarrow H_2O_{2(a)} + Mn^{2+} + O_{2(a)}$	1×10^{7}	0
A39	$Mn^{2+} + OH_{(a)} \rightarrow Mn^{3+} + OH^{-}$	3.4×10^{7}	0
A40	$2\ MnO_2^{+} + 2H^{+} \rightarrow 2Mn^{2+} + H_2O_{2(a)}$	6×10^{6}	0
A41	$MnO^{2+} + 2H^{+} + Mn^{2+} \rightarrow 2Mn^{3+}$	1×10^{5}	0
A42	$Mn^{2+} + O_{3(a)} + H^{+} \rightarrow Mn^{3+} + O_{2(a)} + OH_{(a)}$	1.65×10^{5}	0
A43	$Mn^{2+} + NO_{3(a)} \rightarrow Mn^{3+} + NO_3^{-}$	1.5×10^{6}	0
A44	$Mn^{2+} + HSO_5^{-} \rightarrow Mn^{3+} + SO_4^{-} + OH^{-}$	3×10^{4}	0
A45	$Mn^{2+} + SO_5^{-} \rightarrow Mn^{3+} + HSO_5^{-} + OH^{-}$	1×10^{10}	0
A46	$Mn^{2+} + SO_4^{-} \rightarrow Mn^{3+} + SO_4^{2-}$	1.4×10^{7}	4089
A47	$MnHSO_3^{+} + Mn^{3+} \rightarrow H^{+} + 2Mn^{2+} + SO_3^{-}$	1.3×10^{6}	0
Cu-Fe-Mn redox reactions			
A48	$Cu^{+} + Fe^{3+} \rightarrow Cu^{2+} + Fe^{2+}$	1.3×10^{7}	0
A49	$Cu^{+} + FeOH^{2+} \rightarrow Cu^{2+} + Fe^{2+} + OH^{-}$	1.3×10^{7}	0
A50	$Cu^{+} + Fe(OH)_2^{+} \rightarrow Cu^{2+} + Fe^{2+} + 2\ OH^{-}$	1.3×10^{7}	0
A51	$Mn^{3+} + Fe^{2+} \rightarrow Mn^{2+} + Fe^{3+}$	1.6×10^{4}	0
A52	$Mn^{2+} + FeO^{2+} + 2H^{+} \rightarrow Mn^{3+} + Fe^{3+}$	1×10^{4}	2562
Hydroxide redox reactions			
A53	$O_2^{-} + O_{3(a)} \rightarrow O_{2(a)} + O_3^{-}$	1.5×10^{9}	2200

A54	$2\ HO_{2(a)} \rightarrow H_2O_{2(a)} + O_{2(a)}$	8.3×10^{5}	2700
A55	$HO_{2(a)} + O_2^- + H_2O_{(a)} \rightarrow H_2O_{2(a)} + O_{2(a)} + OH^-$	9.7×10^{7}	1060
A56	$HO_{2(a)} + OH_{(a)} \rightarrow O_{2(a)} + H_2O_{(a)}$	1×10^{10}	0
A57	$O_2^- + OH_{(a)} \rightarrow O_{2(a)} + OH^-$	1.1×10^{10}	2120
A58	$H_2O_{2(a)} + OH_{(a)} \rightarrow HO_{2(a)} + H_2O_{(a)}$	3×10^{7}	1680
Organic reactions			
A59	$H_2C_2O_4 + OH_{(a)} \rightarrow H_2O_{(a)} + C_2O_4^- + H^+$	1.9×10^{8}	2800
A60	$C_2O_4^{2-} + OH_{(a)} \rightarrow OH^- + C_2O_4^-$	1.6×10^{8}	4300
A61	$C_2O_4^- + O_{2(a)} \rightarrow 2\ CO_{2(a)} + O_2^-$	2×10^{9}	2800
A62	$HC_2O_4^- + SO_5^- \rightarrow C_2O_4^- + HSO_5^-$	5×10^{3}	0
A63	$HC_2O_4^- + SO_4^- \rightarrow C_2O_4^- + H^+ + SO_4^{2-}$	3.35×10^{5}	0
A64	$HC_2O_4^- + NO_{3(a)} \rightarrow C_2O_4^- + H^+ + NO_3^-$	6.8×10^{7}	0
A65	$C_2O_4^{2-} + H^+ + SO_5^- \rightarrow C_2O_4^- + HSO_5^-$	1×10^{4}	0
A66	$C_2O_4^{2-} + SO_4^- \rightarrow C_2O_4^- + SO_4^{2-}$	1.05×10^{6}	0
A67	$C_2O_4^{2-} + NO_{3(a)} \rightarrow C_2O_4^- + NO_3^-$	2.2×10^{8}	0
A68	$HCOOH+OH\ (+O_2) \rightarrow$ Products	3.2×10^{9}	0
Fe-oxalate complex reactions			
A69	$Fe^{2+} + C_2O_4^{2-} \rightarrow FeC_2O_{4(a)}$	1×10^{6}	0
A70	$FeC_2O_{4(a)} \rightarrow Fe^{2+} + C_2O_4^{2-}$	1×10^{3}	0
A71	$FeC_2O_4^+ + O_2^- \rightarrow FeC_2O_{4(a)} + O_{2(a)}$	1×10^{6}	0
A72	$FeC_2O_4^+ + HO_{2(a)} \rightarrow FeC_2O_{4(a)} + O_{2(a)} + H^+$	1.2×10^{5}	0
Sulfur and Nitrate compound reactions			
A73	$HSO_3^- + OH_{(a)} \rightarrow SO_3^- + H_2O_{(a)}$	2.7×10^{9}	0
A74	$OH_{(a)} + SO_3^{2-} \rightarrow OH^- + SO_3^-$	4.6×10^{9}	0
A75	$H_2O_{(a)} + N_2O_{5(a)} \rightarrow 2\ H^+ + 2\ NO_3^-$	5×10^{9}	0
A76	$N_2O_{5(a)} \rightarrow NO_2^+ + NO_3^-$	1×10^{9}	0
A77	$H_2O_{(a)} + NO_2^+ \rightarrow 2\ H^+ + NO_3^-$	8.9×10^{7}	0
A78	$Fe^{2+} + NO_{3(a)} \rightarrow Fe^{3+} + NO_3^-$	8×10^{6}	0
A79	$H_2O_{2(a)} + NO_{3(a)} \rightarrow HO_{2(a)} + H^+ + NO_3^-$	4.9×10^{6}	2000
A80	$HO_{2(a)} + NO_{3(a)} \rightarrow H^+ + NO_3^- + O_{2(a)}$	3×10^{9}	0

A81	$NO_{3(a)} + O_2^- \rightarrow NO_3^- + O_{2(a)}$	3×10^{9}	0
A82	$HSO_3^- + NO_{3(a)} \rightarrow H^+ + NO_3^- + SO_3^-$	1.3×10^{9}	2000
A83	$NO_{3(a)} + SO_3^{2-} \rightarrow NO_3^- + SO_3^-$	3×10^{8}	0
A84	$HSO_4^- + NO_{3(a)} \rightarrow H^+ + NO_3^- + SO_4^-$	2.6×10^{5}	0
A85	$NO_{3(a)} + SO_4^{2-} \rightarrow NO_3^- + SO_4^-$	1×10^{5}	0
A86	$NO_{2(a)} + OH_{(a)} \rightarrow HOONO_{(a)}$	1.2×10^{10}	0
A87	$NO_{2(a)} + O_2^- \rightarrow NO_2^- + O_{2(a)}$	1×10^{8}	0
A88	$2\ NO_{2(a)} + H_2O_{(a)} \rightarrow HNO_{2(a)} + H^+ + NO_3^-$	8.4×10^{7}	-2900
A89	$NO_2^- + OH_{(a)} \rightarrow NO_{2(a)} + OH^-$	9.1×10^{9}	0
A90	$NO_2^- + SO_4^- \rightarrow NO_{2(a)} + SO_4^{2-}$	7.2×10^{8}	0
A91	$NO_2^- + NO_{3(a)} \rightarrow NO_{2(a)} + NO_3^-$	1.4×10^{9}	0
A92	$NO_2^- + O_{3(a)} \rightarrow NO_3^- + O_{2(a)}$	5×10^{5}	6900
A93	$HNO_{2(a)} + OH_{(a)} \rightarrow NO_{2(a)} + H_2O_{(a)}$	1.1×10^{10}	0
A94	$HNO_{4(a)} + HSO_3^- \rightarrow HSO_4^- + H^+ + NO_3^-$	3.3×10^{5}	0
A95	$H_2O_{(a)} + SO_{3(a)} \rightarrow 2\ H^+ + SO_4^{2-}$	1×10^{10}	0
A96	$O_{3(a)} + SO_3^{2-} \rightarrow O_{2(a)} + SO_4^{2-}$	1.5×10^{9}	5280
A97	$2\ SO_5^- \rightarrow O_{2(a)} + S_2O_8^{2-}$	4.8×10^{7}	2600
A98	$2\ SO_5^- \rightarrow O_{2(a)} + 2\ SO_4^-$	2.2×10^{8}	2600
A99	$H^+ + O_2^- + SO_5^- \rightarrow HSO_5^- + O_{2(a)}$	2.34×10^{8}	0
A100	$O_{2(a)} + SO_{3(a)} \rightarrow SO_5^-$	2.5×10^{9}	0
A101	$HSO_3^- + SO_5^- \rightarrow HSO_5^- + SO_3^-$	8.6×10^{3}	0
A102	$HSO_3^- + SO_5^- \rightarrow H^+ + SO_4^- + SO_4^{2-}$	3.6×10^{2}	0
A103	$H^+ + SO_3^{2-} + SO_5^- \rightarrow HSO_5^- + SO_3^-$	2.1×10^{5}	0
A104	$SO_3^{2-} + SO_5^- \rightarrow SO_4^- + SO_4^{2-}$	5.5×10^{5}	0
A105	$HSO_4^- + OH_{(a)} \rightarrow SO_4^- + H_2O_{(a)}$	3.5×10^{5}	0
A106	$2\ SO_4^- \rightarrow S_2O_8^{2-}$	6.1×10^{8}	840
A107	$HSO_3^- + SO_4^- \rightarrow H^+ + SO_3^- + SO_4^{2-}$	5.8×10^{8}	0
A108	$SO_3^{2-} + SO_4^- \rightarrow SO_3^- + SO_4^{2-}$	3.4×10^{8}	1200
A109	$H_2O_{2(a)} + SO_4^- \rightarrow HO_{2(a)} + H^+ + SO_4^{2-}$	1.7×10^{7}	0
A110	$HO_{2(a)} + SO_4^- \rightarrow H^+ + O_{2(a)} + SO_4^{2-}$	3.5×10^{9}	0

A111	$O_2^- + SO_4^- \rightarrow O_{2(a)} + SO_4^{2-}$	3.5×10^9	0
A112	$NO_3^- + SO_4^- \rightarrow NO_{3(a)} + SO_4^{2-}$	5×10^4	0
A113	$OH^- + SO_4^- \rightarrow OH_{(a)} + SO_4^{2-}$	1.4×10^7	0
A114	$H_2O_{(a)} + SO_4^- \rightarrow H^+ + OH_{(a)} + SO_4^{2-}$	11	1100
A115	$HSO_3^- + HSO_5^- + H^+ \rightarrow 3\ H^+ + 2\ SO_4^{2-}$	7.14×10^6	0
A116	$SO_3^{2-} + HSO_5^- + H^+ \rightarrow 2\ H^+ + 2\ SO_4^{2-}$	7.14×10^6	0
A117	$HSO_5^- + OH_{(a)} \rightarrow SO_5^- + H_2O_{(a)}$	1.7×10^7	0
A118	$OH_{(a)} + SO_4^- \rightarrow HSO_5^-$	1×10^{10}	0
A119	$H_2O_{2(a)} + HSO_3^- + H^+ \rightarrow 2\ H^+ + SO_4^{2-} + H_2O_{(a)}$	7.2×10^7	4000
A120	$O_{3(a)} + SO_{2(a)} + H_2O_{(a)} \rightarrow HSO_4^- + H^+ + O_{2(a)}$	2.4×10^4	0
A121	$HSO_3^- + O_{3(a)} \rightarrow SO_4^{2-} + H^+ + O_{2(a)}$	3.7×10^5	5530
A122	$NO_{3(a)} + OH^- \rightarrow NO_3^- + OH_{(a)}$	9.4×10^7	2700

155

Table S6. Photolysis rates (aqueous phase) used in the model at noon (sza = 20°)

Number	Reaction	J_0 (s^{-1})
J1	$H_2O_{2(a)} + h\nu \rightarrow 2\ OH_{(a)}$	6.98×10^{-6}
J2	$Fe^{3+} + H_2O_{(a)} + h\nu \rightarrow Fe^{2+} + OH_{(a)} + H^+$	9.3×10^{-6}
J3	$Fe(OH)^{2+} + h\nu \rightarrow Fe^{2+} + OH_{(a)}$	4.39×10^{-3}
J4	$Fe(OH)_2^+ + h\nu \rightarrow Fe^{2+} + OH_{(a)} + OH^-$	5.63×10^{-3}
J5	$NO_2^- + h\nu \rightarrow NO_{(a)} + OH_{(a)}$	2.51×10^{-5}
J6	$NO_3^- + h\nu \rightarrow NO_{2(a)} + OH_{(a)}$	4.15×10^{-7}
J7	$Fe[(C_2O_4)_2]^- + h\nu \rightarrow C_2O_4^{2-} + C_2O_4^- + Fe^{2+}$	2.30×10^{-2}
J8	$Fe[(C_2O_4)_3]^{3-} + h\nu \rightarrow 2\ C_2O_4^{2-} + C_2O_4^- + Fe^{2+}$	5.76×10^{-2}
J9	$FeC_2O_4^+ + h\nu \rightarrow\ Fe^{2+} + C_2O_4^-$	7.20×10^{-4}
J10	$NO_{3(a)} + h\nu \rightarrow NO_{(a)} + O_{2(a)}$	2.32×10^{-2} *
J11	$NO_{3(a)} + h\nu \rightarrow NO_{2(a)} + O_{(a)}^{3p}$	2.01×10^{-1} *

*Estimated as in the gas phase

160 Table S7. Aqueous equilibrium reactions

Number	Reaction	K_{298} (M)	k_{298} (M^{-n} s^{-1}) forward	E_a/R (K)	k_{298} (M^{-n} s^{-1}) backward	E_a/R (K)
E1	$H_2O_{(a)} \leftrightarrow H^+ + OH^-$	1.8×10^{-16}	2.34×10^{-5}	6800	1.3×10^{11}	0
E2	$NH_{3(a)} + H_2O_{(a)} \leftrightarrow NH_4^+ + OH^-$	1.17×10^{-5}	6.02×10^{5}	560	3.4×10^{10}	
E3	$HO_{2(a)} \leftrightarrow H^+ + O_2^-$	1.6×10^{-5}	8.0×10^{5}	0	5×10^{10}	0
E4	$HNO_{3(a)} \leftrightarrow H^+ + NO_3^-$	22	1.1×10^{12}	-1800	5×10^{10}	
E5	$HNO_{2(a)} \leftrightarrow H^+ + NO_2^-$	5.30×10^{-4}	2.65×10^{7}	1760	5×10^{10}	
E6	$HNO_{4(a)} \leftrightarrow H^+ + O_2NO_2^-$	1×10^{-5}	5×10^{5}		5×10^{10}	
E7	$HO_{2(a)} + NO_{2(a)} \leftrightarrow HNO_{4(a)}$	2.17×10^{9}	1×10^{7}		4.6×10^{-3}	
E8	$HO_{2(a)} + SO_{2(a)} \leftrightarrow HSO_3^- + H^+$	3.14×10^{-4}	6.27×10^{4}	-1940	2.0×10^{8}	
E9	$HSO_3^- \leftrightarrow H^+ + SO_3^{2-}$	6.22×10^{-8}	3110	-1960	5×10^{10}	
E10	$H_2SO_{4(a)} \leftrightarrow HSO_4^- + H^+$	1×10^{3}	5×10^{13}		5×10^{10}	
E11	$HSO_4^- \leftrightarrow H^+ + SO_4^{2-}$	1.02×10^{-2}	1.02×10^{9}	-2700	1×10^{11}	
E12	$Fe^{3+} + H_2O_{(a)} \leftrightarrow Fe(OH)^{2+} + H^+$	1.09×10^{-4}	4.7×10^{4}		4.3×10^{8}	
E13	$Fe(OH)^{2+} + H_2O_{(a)} \leftrightarrow Fe(OH)_2^+ + H^+$	1.38×10^{-7}	1.1×10^{3}		8×10^{9}	
E14	$Fe^{3+} + SO_4^{2-} \leftrightarrow Fe(SO_4)^+$	1.78×10^{-2}	3.2×10^{3}		1.8×10^{5}	
E15	$Cu^{2+} + OH_{(a)} \leftrightarrow Cu(OH)^{2+}$	1.17×10^{4}	3.5×10^{8}		3×10^{4}	
E16	$HO_{3(a)} \leftrightarrow H^+ + O_3^-$	5×10^{-9}	330		5.2×10^{10}	
E17	$HOONO_{(a)} \leftrightarrow H^+ + OONO^-$	1×10^{-6}	5×10^{4}		5×10^{10}	
E18	$Fe(C_2O_4)^+ \leftrightarrow C_2O_4^{2-} + Fe^{3+}$	4.0×10^{-10}	3×10^{-3}		7.5×10^{6}	
E19	$Fe(C_2O_4)_2^- \leftrightarrow C_2O_4^{2-} + Fe(C_2O_4)^+$	1.59×10^{-7}	3×10^{-3}		1.89×10^{4}	
E20	$Fe(C_2O_4)_3^{3-} \leftrightarrow C_2O_4^{2-} + Fe(C_2O_4)_2^-$	2.65×10^{-5}	3×10^{-3}		114	

Table S8. Kinetic data for the simulation of gas-liquid phase conversion reactions

Number	Reaction*	k_{298} (M^{-n+1} s^{-1}) forward	k_{298} (M^{-n+1} s^{-1}) backward
T1	$CO_{2(g)} \leftrightarrow CO_{2(a)}$	$k_{mt\ CO2}$×ALWC	$k_{mt\ CO2}/(H_{CO2}RT)$
T2	$NH_{3(g)} \leftrightarrow NH_{3(a)}$	$k_{mt\ NH3}$×ALWC	$k_{mt\ NH3}/(H_{NH3}RT)$
T3	$O_{3(g)} \leftrightarrow O_{3(a)}$	$k_{mt\ O3}$×ALWC	$k_{mt\ O3}/(H_{O3}RT)$
T4	$HO_{2(g)} \leftrightarrow HO_{2(a)}$	$k_{mt\ HO2}$×ALWC	$k_{mt\ HO2}/(H_{HO2}RT)$
T5	$OH_{(g)} \leftrightarrow OH_{(a)}$	$k_{mt\ OH}$×ALWC	$k_{mt\ OH}/(H_{OH}RT)$
T6	$H_2O_{2(g)} \leftrightarrow H_2O_{2(a)}$	$k_{mt\ H2O2}$×ALWC	$k_{mt\ H2O2}/(H_{H2O2}RT)$
T7	$NO_{3(g)} \leftrightarrow NO_{3(a)}$	$k_{mt\ NO3}$×ALWC	$k_{mt\ NO3}/(H_{NO3}RT)$
T8	$N_2O_{5(g)} \leftrightarrow N_2O_{5(a)}$	$k_{mt\ N2O5}$×ALWC	$k_{mt\ N2O5}/(H_{N2O5}RT)$
T9	$NO_{2(g)} \leftrightarrow NO_{2(a)}$	$k_{mt\ NO2}$×ALWC	$k_{mt\ NO2}/(H_{NO2}RT)$
T10	$SO_{2(g)} \leftrightarrow SO_{2(a)}$	$k_{mt\ SO2}$×ALWC	$k_{mt\ SO2}/(H_{SO2}RT)$

*k_{mt} is related to the particle diameters and the aerosol liquid water in different diameter bins. For this reason, the mass transfer rates are corrected by the particle 11 bins diameters in the two field campaigns. The rate k_{mt} equals to $\sum_i^{11} k_{mt\_i} \times L_i$

Table S9. Concentration of transition metals in $PM_{2.5}$ in urban areas.

Sampling site	Period	Method	Fe	Mn	Cu	References
China, Beijing, Urban	2018.8-2019.8	XRF	596	27.9	7.37	Zhao et al. (2021)
China, Beijing, Urban	2015.9-2016.1	XRF	686	60.2	25.1	Zhang et al. (2019)
China, Beijing, Urban	2016.6-2017.5	ED-XRF	738	37	32	Cui et al. (2019)
China, Beijing, Urban	2014.1-10	ICP-AES	1650	55	108	Gao et al. (2018)
China, Beijing, Urban	2016.1-2017.5	XRF	629	32	24	Cui et al. (2020)
China, Beijing, Urban	2016.1	ICP-AES	2823	92.3	48	Duan et al. (2012)
China, Zhengzhou, Urban	2017.10-2018.7	XRF	1361	157	29.2	He et al. (2019)
China, Nanjing, Urban	2016.12-2017.12	XRF	577	48.9	27.2	Yu et al. (2019)
China, Shanghai, Urban	2016.3-2017.2	ED-XRF	410	32	12	Chang et al. (2017)
Canada, Hamilton, Urban	2014.1-2017.6	XRF	49.6	0.83	2.76	Sofowote et al. (2019)
India, New Delhi, Urban	2013.1-2016.12	WD-XRF	780	10	100	Jain et al. (2020)

SI References

Ali, H. M., Iedema, M., Yu, X.-Y., and Cowin, J. P.: Ionic strength dependence of the oxidation of SO2 by H2O2 in sodium chloride particles, Atmospheric Environment, 89, 731-738, 2014.

Beltran, F. J.: Ozone reaction kinetics for water and wastewater systems, crc Press, 2003.

Burkholder, J., Sander, S., Abbatt, J., Barker, J., Cappa, C., Crounse, J., Dibble, T., Huie, R., Kolb, C., and Kurylo, M.: Chemical kinetics and photochemical data for use in atmospheric studies; evaluation number 19, Pasadena, CA: Jet Propulsion Laboratory, National Aeronautics and Space …, 2020.

Chang, Y., Huang, K., Deng, C., Zou, Z., Liu, S., and Zhang, Y.: First long-term and near real-time measurement of atmospheric trace elements in Shanghai, China, Atmos. Chem. Phys. Discuss., in Review, 2017.

Cheng, Y., Zheng, G., Wei, C., Mu, Q., Zheng, B., Wang, Z., Gao, M., Zhang, Q., He, K., and Carmichael, G.: Reactive nitrogen chemistry in aerosol water as a source of sulfate during haze events in China, Science Advances, 2, e1601530, 2016a.

Cheng, Y., Zheng, G., Wei, C., Mu, Q., Zheng, B., Wang, Z., Gao, M., Zhang, Q., He, K., Carmichael, G., Pöschl, U., and Su, H.: Reactive nitrogen chemistry in aerosol water as a source of sulfate during haze events in China, Science Advances, 2, e1601530, 10.1126/sciadv.1601530, 2016b.

Chung, M. Y., Muthana, S., Paluyo, R. N., and Hasson, A. S.: Measurements of effective Henry's law constants for hydrogen peroxide in concentrated salt solutions, Atmospheric Environment, 39, 2981-2989, 2005.

Clegg, S., Kleeman, M., Griffin, R., and Seinfeld, J.: Effects of uncertainties in the thermodynamic properties of aerosol components in an air quality model–Part 1: Treatment of inorganic electrolytes and organic compounds in the condensed phase, Atmospheric Chemistry and Physics, 8, 1027-1085, 2008.

Clever, H. L.: Setchenov salt-effect parameter, Journal of Chemical and Engineering Data, 28, 340-343, 1983.

Clifton, C. L., Altstein, N., and Huie, R. E.: Rate constant for the reaction of nitrogen dioxide with sulfur (IV) over the pH range 5.3-13, Environmental science & technology, 22, 586-589, 1988.

Cui, Y., Ji, D., Chen, H., Gao, M., Maenhaut, W., He, J., and Wang, Y.: Characteristics and sources of hourly trace elements in airborne fine particles in urban Beijing, China, Journal of Geophysical Research: Atmospheres, 124, 11595-11613, 2019.

Cui, Y., Ji, D., He, J., Kong, S., and Wang, Y.: In situ continuous observation of hourly elements in PM2. 5 in urban beijing, China: Occurrence levels, temporal variation, potential source regions and health risks, Atmospheric Environment, 222, 117164, 2020.

Duan, J. C., Tan, J. H., Wang, S. L., Hao, J. M., and Chail, F. H.: Size distributions and sources of elements in particulate matter at curbside, urban and rural sites in Beijing, Journal of Environmental Sciences, 24, 87-94, 10.1016/s1001-0742(11)60731-6, 2012.

Fountoukis, C., and Nenes, A.: ISORROPIA II: a computationally efficient thermodynamic equilibrium model for K^+-Ca^{2+}-Mg^{2+}-NH_4^+-Na^+-SO_4^{2-}-NO_3^--Cl^--H2O aerosols, Atmospheric Chemistry and Physics, 7, 4639-4659, 2007a.

Fountoukis, C., and Nenes, A.: ISORROPIA II: a computationally efficient thermodynamic equilibrium model for K^+-Ca^{2+}-Mg^{2+}-NH_4^+-Na^+-SO_4^{2-}-NO_3^--Cl^--H2O aerosols, Atmospheric Chemistry and Physics Discussions, 7, 1893-1939, 2007b.

Gao, J., Wang, K., Wang, Y., Liu, S., Zhu, C., Hao, J., Liu, H., Hua, S., and Tian, H.: Temporal-spatial characteristics and source apportionment of PM2. 5 as well as its associated chemical species in the Beijing-Tianjin-Hebei region of China, Environmental Pollution, 233, 714-724, 2018.

Guo, H., Weber, R. J., and Nenes, A.: High levels of ammonia do not raise fine particle pH sufficiently to yield nitrogen oxide-dominated sulfate production, Scientific Reports, 7, 12109, 10.1038/s41598-017-11704-0, 2017.

He, R.-D., Zhang, Y.-S., Chen, Y.-Y., Jin, M.-J., Han, S.-J., Zhao, J.-S., Zhang, R.-Q., and Yan, Q.-S.: Heavy metal pollution characteristics and ecological and health risk assessment of atmospheric PM2. 5 in a living area of Zhengzhou City, Huan jing ke xue= Huanjing kexue, 40, 4774-4782, 2019.

Herrmann, H., Schaefer, T., Tilgner, A., Styler, S. A., Weller, C., Teich, M., and Otto, T.: Tropospheric Aqueous-Phase Chemistry: Kinetics, Mechanisms, and Its Coupling to a Changing Gas Phase, Chemical Reviews, 115, 4259-4334, 10.1021/cr500447k, 2015.

Huss Jr, A., Lim, P. K., and Eckert, C.: Oxidation of aqueous sulfur dioxide. 1. Homogeneous manganese (II) and iron (II) catalysis at low pH, The Journal of Physical Chemistry, 86, 4224-4228, 1982.

Ibusuki, T., and Takeuchi, K.: Sulfur dioxide oxidation by oxygen catalyzed by mixtures of manganese(II) and iron(III) in aqueous solutions at environmental reaction conditions, Atmospheric Environment (1967), 21, 1555-1560, https://doi.org/10.1016/0004-6981(87)90317-9, 1987.

Jain, S., Sharma, S., Vijayan, N., and Mandal, T.: Seasonal characteristics of aerosols (PM2. 5 and PM10) and their source apportionment using PMF: a four year study over Delhi, India, Environmental Pollution, 262, 114337, 2020.

Kontogeorgis, G. M., Maribo-Mogensen, B., and Thomsen, K.: The Debye-Hückel theory and its importance in modeling electrolyte solutions, Fluid Phase Equilibria, 462, 130-152, 2018.

Kosak-Channing, L. F., and Helz, G. R.: Solubility of ozone in aqueous solutions of 0-0.6 M ionic strength at 5-30. degree. C, Environmental science & technology, 17, 145-149, 1983.

Lagrange, J., Pallares, C., Wenger, G., and Lagrange, P.: Electrolyte effects on aqueous atmospheric oxidation of sulphur dioxide by hydrogen peroxide, Atmospheric Environment. Part A. General Topics, 27, 129-137, https://doi.org/10.1016/0960-1686(93)90342-V, 1993.

Lee, Y., and Schwartz, S. E.: Kinetics of oxidation of aqueous sulfur (IV) by nitrogen dioxide, Precipitation Scavenging, Dry Deposition and Resuspension, 1, 453-470, 1983.

Li, J., Polka, H.-M., and Gmehling, J.: A gE model for single and mixed solvent electrolyte systems: 1. Model and results for strong electrolytes, Fluid Phase Equilibria, 94, 89-114, 1994.

Linder, P. W., and Murray, K.: Correction of formation constants for ionic strength, from only one or two data points: An examination of the use of the extended Debye—Hückel equation, Talanta, 29, 377-382, 1982.

Liu, M., Song, Y., Zhou, T., Xu, Z., Yan, C., Zheng, M., Wu, Z., Hu, M., Wu, Y., and Zhu, T.: Fine particle pH during severe haze episodes in northern China, Geophysical Research Letters, 44, 5213-5221, https://doi.org/10.1002/2017GL073210, 2017.

Liu, T., Clegg, S. L., and Abbatt, J. P. D.: Fast oxidation of sulfur dioxide by hydrogen peroxide in deliquesced aerosol particles, Proceedings of the National Academy of Sciences, 117, 1354-1359, 10.1073/pnas.1916401117, 2020.

Maahs, H. G.: Kinetics and mechanism of the oxidation of S(IV) by ozone in aqueous solution with particular reference to SO2 conversion in nonurban tropospheric clouds, Journal of Geophysical Research: Oceans, 88, 10721-10732, https://doi.org/10.1029/JC088iC15p10721, 1983.

Maaß, F., Elias, H., and Wannowius, K. J.: Kinetics of the oxidation of hydrogen sulfite by hydrogen peroxide in aqueous solution:: ionic strength effects and temperature dependence, Atmospheric Environment, 33, 4413-4419, 1999.

Martin, L. R., and Hill, M. W.: The iron catalyzed oxidation of sulfur: Reconciliation of the literature rates, Atmospheric Environment (1967), 21, 1487-1490, 1967.

Martin, L. R., and Hill, M. W.: The effect of ionic strength on the manganese catalyzed oxidation of sulfur (IV), Atmospheric Environment (1967), 21, 2267-2270, 1987.

McArdle, J. V., and Hoffmann, M. R.: Kinetics and mechanism of the oxidation of aquated sulfur dioxide by hydrogen peroxide at low pH, The Journal of Physical Chemistry, 87, 5425-5429, 1983.

Millero, F. J., Hershey, J. B., Johnson, G., and Zhang, J.-Z.: The solubility of SO 2 and the dissociation of H 2 SO 3 in NaCl solutions, J Atmos Chem, 8, 377-389, 1989.

Ming, Y., and Russell, L. M.: Thermodynamic equilibrium of organic-electrolyte mixtures in aerosol particles, AIChE Journal, 48, 1331-1348, 2002.

Pitzer, K. S.: Ion interaction approach: theory and data correlation, Activity coefficients in electrolyte solutions, 2, 75-153, 1991.

Polka, H.-M., Li, J., and Gmehling, J.: A gE model for single and mixed solvent electrolyte systems: 2. Results and comparison with other models, Fluid phase equilibria, 94, 115-127, 1994.

Raatikainen, T., and Laaksonen, A.: Application of several activity coefficient models to water-organic-electrolyte aerosols of atmospheric interest, 2005.

Rischbieter, E., Stein, H., and Schumpe, A.: Ozone solubilities in water and aqueous salt solutions, Journal of Chemical & Engineering Data, 45, 338-340, 2000.

Ross, H. B., and Noone, K. J.: A numerical investigation of the destruction of peroxy radical by Cu ion catalyzed-reactions of atmospheric particles, J Atmos Chem, 12, 121-136, 10.1007/bf00115775, 1991.

Rusumdar, A., Wolke, R., Tilgner, A., and Herrmann, H.: Treatment of non-ideality in the SPACCIM multiphase model-Part 1: Model development, 2016.

Rusumdar, A. J., Tilgner, A., Wolke, R., and Herrmann, H.: Treatment of non-ideality in the SPACCIM multiphase model – Part 2: Impacts on the multiphase chemical processing in deliquesced aerosol particles, Atmos. Chem. Phys., 20, 10351-10377, 10.5194/acp-20-10351-2020, 2020.

Seinfeld, J. H., and Pandis, S. N.: Atmospheric chemistry and physics: from air pollution to climate change, John Wiley & Sons, 2016.

Sofowote, U. M., Di Federico, L. M., Healy, R. M., Debosz, J., Su, Y., Wang, J., and Munoz, A.: Heavy metals in the near-road environment: Results of semi-continuous monitoring of ambient particulate matter in the greater Toronto and Hamilton area, Atmospheric Environment: X, 1, 100005, 2019.

Wang, X., Gemayel, R., Hayeck, N., Perrier, S., Charbonnel, N., Xu, C., Chen, H., Zhu, C., Zhang, L., Wang, L., Nizkorodov, S. A., Wang, X., Wang, Z., Wang, T., Mellouki, A., Riva, M., Chen, J., and George, C.: Atmospheric Photosensitization: A New Pathway for Sulfate Formation, Environmental Science & Technology, 54, 3114-3120, 10.1021/acs.est.9b06347, 2020.

Yu, Y., He, S., Wu, X., Zhang, C., Yao, Y., Liao, H., Wang, Q. g., and Xie, M.: PM2. 5 elements at an urban site in Yangtze River Delta, China: High time-resolved measurement and the application in source apportionment, Environmental Pollution, 253, 1089-1099, 2019.

Zhang, B., Zhou, T., Liu, Y., Yan, C., Li, X., Yu, J., Wang, S., Liu, B., and Zheng, M.: Comparison of water-soluble inorganic ions and trace metals in $PM_{2.5}$ between online and offline measurements in Beijing during winter, Atmospheric Pollution Research, 10, 1755-1765, https://doi.org/10.1016/j.apr.2019.07.007, 2019.

Zhao, S., Tian, H., Luo, L., Liu, H., Wu, B., Liu, S., Bai, X., Liu, W., Liu, X., Wu, Y., Lin, S., Guo, Z., Lv, Y., and Xue, Y.: Temporal variation characteristics and source apportionment of metal elements in PM2.5 in urban Beijing during 2018–2019, Environmental Pollution, 268, 115856, https://doi.org/10.1016/j.envpol.2020.115856, 2021.

Zheng, H., Song, S., Sarwar, G., Gen, M., Wang, S., Ding, D., Chang, X., Zhang, S., Xing, J., Sun, Y., Ji, D., Chan, C. K., Gao, J., and McElroy, M. B.: Contribution of Particulate Nitrate Photolysis to Heterogeneous Sulfate Formation for Winter Haze in China, Environmental Science & Technology Letters, 7, 632-638, 10.1021/acs.estlett.0c00368, 2020.

Zuend, A., Marcolli, C., Luo, B. P., and Peter, T.: A thermodynamic model of mixed organic-inorganic aerosols to predict activity coefficients, 2008.

Zuend, A., Marcolli, C., Booth, A., Lienhard, D. M., Soonsin, V., Krieger, U., Topping, D. O., McFiggans, G., Peter, T., and Seinfeld, J. H.: New and extended parameterization of the thermodynamic model AIOMFAC: calculation of activity coefficients for organic-inorganic mixtures containing carboxyl, hydroxyl, carbonyl, ether, ester, alkenyl, alkyl, and aromatic functional groups, Atmospheric Chemistry and Physics, 11, 9155-9206, 2011.